Journal of Materials Chemistry A

Accepted Manuscript

ROYAL SOCIETY OF CHEMISTRY

www.rsc.org/materialsA

Cite this: DOI: 10.1039/c0xx00000x

www.rsc.org/xxxxxx

ARTICLE TYPE

Facile upscale synthesis of Layered iron oxide Nanosheets and its Application for Phosphate Removal

Liping Fang*[a,b,c], Lizhi Huang[b], Peter E. Holm[b,c], Xiaofang Yang[d], Hans Christian B. Hansen[b,c], Dongsheng, Wang*[d]

Received (in XXX, XXX) Xth XXXXXXXXX 20XX, Accepted Xth XXXXXXXXX 20XX
DOI: 10.1039/b000000x

Layered iron oxide (Fe^{III}) nanosheets are new efficient adsorbent which are here developed and investigated for removing eutrophication pollutant phosphate from water. The layered Fe^{III} nanosheets are synthesized by anion exchanging layered Fe^{II}/Fe^{III} hydroxide chloride (green rust; GR) with dodecanoate, followed by solid state oxidation and exfoliation, with which the yield of the product can be easily scaled up. The obtained product exhibits distinct platy structure with a minimal plate thickness of 1 nm and lateral size of 100 to 200 nm referring to 1 to 2 layers of the Fe^{III} nanosheets by means of high resolution transmission electronic microscopy, selected area electronic diffraction and atomic force microscopy. The Fe^{III} nanosheets can be well dispersed and stable in aqueous solution, showing low tendency of aggregation. The performance of the obtained nanosheets to remove phosphate has been evaluated in kinetic and batch experiments under different environmental conditions (i.e. interfering anions and pH). The kinetic study shows that phosphate removal by the iron oxide quickly reaches plateau with an adsorption constant k_2 ranging from 5.2×10^{-4} to 1.4×10^{-3} g/(μmol min) for the initial phosphate concentrations of 40 and 80 μmol/L (1.2 to 2.4 mg P/L) at pH 7. The maximum phosphate adsorption capacity of the layered Fe^{III} nanosheets is 2540 μmol/g (about 77 mg/g; 4006 μmol P/g Fe) at pH 5, showing excellent potential for phosphate removal from wastewater. Our results also indicate that the performance of the layered Fe^{III} nanosheets for phosphate removal is highly selective. X-ray photoelectron spectroscopic analyses of O 1s, Fe 2p and P 2p spectra provide evidences showing that the iron oxide nanosheets removes phosphate by forming inner-sphere Fe-O-P complexes rather than Fe-P. The cost-effective, environmental friendly and highly efficient layered Fe^{III} nanosheets material is a promising material to be used for phosphate removal or other oxyanions in future water treatment technologies.

1. Introduction

Phosphorus is an essential nutrient for all living organisms, and as such phosphorus is present in all parts of ecosystems, not at least food production systems. Phosphorus is mainly discharged as form of phosphate into aquatic environments from soils, sediments, industries and via wastes from households [1]. Excess levels of phosphorus will cause severe adverse effect to ecosystem, such as eutrophication of lakes, lagoon and rivers. Concurrently, phosphorus is also a limited resource that needs to be captured and reused. Thus, phosphorus recovery from the aquatic environment does not only prevent the loss of nutrient resources, but also eliminate serious environmental problem. Various physicochemical approaches have been developed to recover phosphate from wastewater, such as precipitation, crystallization, anion exchange, and sorption [1-6]. Typically, in virtue of advanced nanotechnology, a number of nanomaterials with unique structures have been developed and exhibiting excellent efficiency for removing phosphate [4-6].

As a class of anionic clays, layered double hydroxides (LDHs) comprise positively charged trioctahedral metal hydroxide layers and interlayer anions with a general formula of $[M^{II}_{(1-x)}M^{III}_{x}(OH)_2](A^{n-})_{x/n}\cdot mH_2O$, where M^{II} and M^{III} denote di- and tri-valent metal ions, A^{n-} is the counter anion and m is the number of water molecules between the metal hydroxide layers [7-9]. The positively charged metal hydroxide layers can be considered as a partial substitution of divalent cations (M^{II}) in brucite-like (*i.e.* $Mg(OH)_2$) structure by trivalent cations (M^{III}), and charge balanced by intercalation of various anions (A^{n-}) [10]. The feature of the positively charged brucite-like sheets and relatively weak bonding of interlayer anions offers LDHs strong anion exchange and adsorption capacities, showing high prospect for removing various oxyanion pollutants in water treatment [11]. LDHs are considered as efficient adsorbents to remove phosphate with adsorption capacities ranging from 16 to 47 mg P/g [3, 11-13]. Studies show that the adsorption capacity of LDHs is notably determined by the nature and content of cations located in layers [11, 14]. For example, the increase of trivalent Al ions or the addition of tetravalent Zr in layers can significantly enhance phosphate removal [1, 15], whereas, this can increase the release of ecotoxic element such as Al releasing into aquatic environment, consequently threatening the safety of organisms [11]. Meanwhile, the performance of LDHs is also affected by the feature of interlayer anions due to their different affinities with brucite-like layers, for example, previous study shows that NO_3^- type Zn/Al LDH exhibits much stronger adsorption for phosphate than that CO_3^{2-} and Cl^- intercalated LDH [16]. Though calcination of LDHs prior to their application in water cleanup can cope with this shortage, the release of those cations from planar layers becomes significantly severe [10-11].

Iron oxides are well known for their strong phosphate binding affinity and capacity, hence, an interesting opportunity is to use iron-rich LDHs as a source of iron oxide [17]. Green rusts (GR) are a class of monometallic iron bearing LDHs (Fe^{II}/Fe^{III} LDHs), which are intermediate products forming during iron oxidization/corrosion. This type of Fe^{II}/Fe^{III} LDH is very active and unstable in air, which can transform to other iron

(hydro)oxides such as goethite (α-FeOOH), lepidocrocite (γ-FeOOH), amorphous ferrihydrite and magnetite depending on the type of anions in the interlayers (e.g. Cl^-, SO_4^{2-}), as a consequence, leading to the poorer adsorption of GRs towards phosphate and other oxyanions [18-19]. Genin and Legrand reported that CO_3^{2-} type GR could convert to "ferric" oxhydroxylcarbonate GR (Fe^{III}/Fe^{III} LDH) via rapid oxidation in H_2O_2, respectively, whereas, the observed evidence of structural transformation based on X-ray and electronic diffractions could not support this hypothesis [20-21]. Recently, we successfully synthesized organic GR interleaved with dodecanoate anions whose structure remained intact and highly crystalline after complete solid state oxidation of Fe^{II} to Fe^{III} in air [22-23]. This Fe^{III}/Fe^{III} LDH can be an ideal choice for phosphate recovery due to the nature of iron oxides to bind phosphate and the unique feature of well dispersion in water solution. However, no such study has been carried out yet. Besides, the yield of this product (Table S1) severely constrains its further application by using current one-pot synthesis method [22]. Moreover, the presence of dodecanoate anions in the interlayers may also be an obstacle for the performance of Fe^{III}/Fe^{III} LDH, which also should be eliminated.

In this study, we developed a new facile approach of upscale synthesis Fe^{III}/Fe^{III} LDH via simple precipitation and oxidation of Fe^{II} ions methods, subsequently, followed by exfoliation of the Fe^{III}/Fe^{III} LDH to the layered Fe^{III} nanosheets by removing hydrophobic dodecanoate anions. The as-synthesized Fe^{III}/Fe^{III} LDH and its exfoliated product were then subject to systematically characterizations. Finally, the as-synthesized Fe^{III}/Fe^{III} LDH and its layered Fe^{III} nanosheets were examined for removing phosphate which is the main phosphorus form found in wastewater with eutrophication issues.

2. Experimental

2.1 Materials

Iron(II) chloride salt ($FeCl_2 \cdot 4H_2O$; purity > 98%) and dodecanoic acid ($C_{12}H_{24}O_2$; purity > 99%) was purchased from Alfa Aesar. All chemicals were of analytical grade, and used without further purification. Milli-Q water (*18.2* MΩ·cm) and ultrapure argon (purity > 99.9995%) were used throughout.

2.2 Synthesis of dodecanoate intercalated Fe^{III}/Fe^{III} LDH

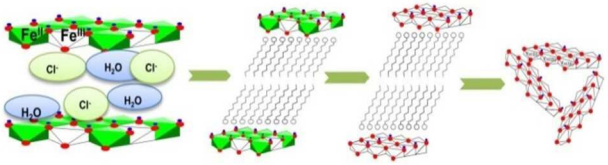

Scheme 1 Schematic illustration of synthesis of the layered Fe^{III} nanosheets

Dodecanoate intercalated Fe^{III}/Fe^{III} LDH (Fe^{III}/Fe^{III} LDH(C12)) was synthesized by solid-state-oxidation of dodecanoate intercalated GR (GR(C12); Fe^{II}:Fe^{III} =3:1) derived from anion exchange of chloride containing green rust (GR(Cl)) with dodecanoate anions (Scheme 1).

GR(Cl) was prepared by partial oxidation of freshly precipitated Ferrous hydroxide ($Fe(OH)_2$) [21]. Briefly, $FeCl_2$ and NaOH solutions were mixed with a $[Fe^{2+}]/[OH^-]$ ratio of 0.7, to obtain a final concentration of 0.36 M for iron (II). This mixed solution (200 mL) was vigorously stirred using a magnetic bar under protection of Ar gas stream at 25 ± 1°C. A rate of 1.5 mL/min O_2 was pumped into the solution during continuous stirring, meanwhile, the pH of the solution simultaneously monitored through the whole reaction. After approximately 1.5 hrs reaction where about 1/4 of total Fe^{II} ions were oxidized to ferric form, the pump was turned off and the greenish-blue suspension was further aged for 24 hrs without exposing to oxygen at room temperature.

The aged GR(Cl) slurry was separated by centrifugation at a speed of 2500 g for 5 min, and dispersed immediately in 500 mL of 0.2 M Ar-bubbled sodium dodecanoate solution (30% ethanol). The glass container was capped with a rubber septum with an in- and outlets to/from flask, which allowed to flush with Ar gas to remove trace oxygen in headspace. Such solution was stirred mildly for 3 days to exchange chloride interlayer anions to dodecanoate anions. The resulting GR(C12) was further washed with Ar-bubbled ethanol and water prior to freeze-drying. Finally, Fe^{III}/Fe^{III} LDH was obtained by exposing the complete dried GR(C12) particles to air for 24 h.

2.3 Exfoliation of Fe^{III}/Fe^{III} LDH to layered nanosheets

The synthesized Fe^{III}/Fe^{III} LDH (1.0 g) was mixed with 1.0 L of MilliQ water in a glass flask using a magnetic bar. The pH was adjusted to 12.7 where the intercalated dodecanoate anions were repelled by the same negatively charged iron hydroxide layers. Such suspension was magnetically stirred for 24 h to acquire a complete exfoliation, consequently, the solution was repeatedly centrifugated and re-dispersed in ethanol to remove dodecanoate anions. The dispersion of Fe^{III} layer nanosheets in MilliQ water was treated using a sonicator coupled with a microtip at 200 W (Ultrasonic processor, Shanghai) for 1 h in an ice bath. To remove large aggregated or unexfoliated particles, the resulting orange colloidal suspension was then centrifugated at 1000 g for 10 min.

2.4 Characterization of the layered Fe^{III} nanosheets and its precursors

The chemical compositions of the products were analyzed by dissolving the proper amounts of the solids in 0.1 M HCl. The Fe^{II} contents within in GR(Cl) and GR(C12) was determined by using a modified phenanthroline method [24], while the content of total Fe was analyzed by using an Optima 8300 inductive coupled plasma optical emission spectrometer (ICP-OES; PerkinElmer, USA). The contents of chloride and dodecanoate ions within the solid were measured by using a Dionex ICS-2100 ion chromatography (IC), and an Agilent 6890 series gas chromatograph equipped with a flame-ionization detector (GC-FID, USA), respectively (Details are given in supplemental document S1).

Evolution of X-ray diffraction for the as-synthesized products from GR(Cl) to exfoliated Fe^{III} layered nanosheets was tracked by a X'Pert PRO MRD diffractometer (PANalytical, Netherlands) coupled with monochromatic Cu Kα radiation (λ = 0.15405 nm). The morphology and size of Fe^{III}/Fe^{III} LDH and its exfoliated nanosheets were examined with a Hitachi S-3000N scanning electronic microscope coupled with a DEAX Energy Dispersive Spectroscopy (SEM/EDS), and a JEOL 2100F transmission electronic microscope (TEM) operating at 200 kV. A Veeco nanoscope IIIa atomic force microscopy system (AFM) was used to analyze topography of the Fe^{III} layered nanosheets in contact mode using a Si-tip cantilever. Fourier transformation infrared spectroscopy (FT-IR) spectra for the samples were obtained by using a Nicolet 8700 (Thermo scientific, USA). The specific Brunauer Emmett Teller (BET) surface area was

characterized by the nitrogen adsorption method using a Micromeritics ASAP2000 Surface Area Analyzer (Micrometitics instrument corporation, USA). 20 mg of powder samples were degassed at room temperature using a vacuum pump for two hours before the measurement. Thermogravimetric analyses (TGA) of the Fe^{III}/Fe^{III} LDH and its exfoliated nanosheets were performed in a Pyris1 TGA (PerkinElmer Instruments, USA) with the temperature set up to 800 °C, and collected at a heating rate of 5 °C/min. Zeta potential of the layered Fe^{III} nanosheets as a function of pH from 3 to 10 was monitored by using a Zetasizer Nano ZS (Malvern, England).

2.5 Removal of phosphate by using Fe^{III} layered nanosheets

Both sorption isotherm and kinetic experiments were used to study removal efficiency of phosphate by the Fe^{III} nanosheets at different pHs. Besides, influence of various co-existed anions (i.e. Cl^-, NO_3^-, SO_4^{2-} and HCO_3^-) on phosphate removal was also addressed. The Fe^{III} nanosheets suspension (0.1- 0.2 g/L as Fe) was obtained via exfoliation process as described above, and used for following sorption experiments.

The sorption kinetics study was performed by spiking appropriate amounts of P stock solution into each 7 mL Fe^{III} nanosheets suspension to acquire an initial P concentration of 40 and 80 μM, respectively. The solution was maintained at pH 7.0 throughout the whole contact period, and the ionic strength was controlled with 0.1 M $NaNO_3$. At each described reaction point (0 to 24 hrs), the supernatant was sampled after an aliquot of 7 mL of phosphate spiked suspension was centrifugated at 3000 g.

The phosphate sorption isotherm experiments were conducted at 25 ± 1°C with an ionic strength of 0.1 M $NaNO_3$. The Fe^{III} nanosheets suspensions were contacted with phosphate with varying initial concentrations of 0 to 1500 μM for 24 hrs at pH 5, 7.5 and 9, respectively. Besides, the competitive sorption of background anions (i.e. Cl^-, NO_3^-, SO_4^{2-} and HCO_3^-) to the Fe^{III} nanosheets was further investigated with different ionic strengths from 0 to 0.5 M at pH 7. The supernatants were collected by centrifugation of the Fe^{III} nanosheets suspensions after 24 hrs equilibration. The phospahte concentrations in supernatants were analyzed by using a molybdate colorimetric (Murphy-Riley) procedure on a U-2900 UV-vis spectrophotometer (Hitachi, Japan) at wavelength of 720 nm [25].

3. Results and discussion

3.1 Synthesis GR(Cl) and anion exchange to GR(C12)

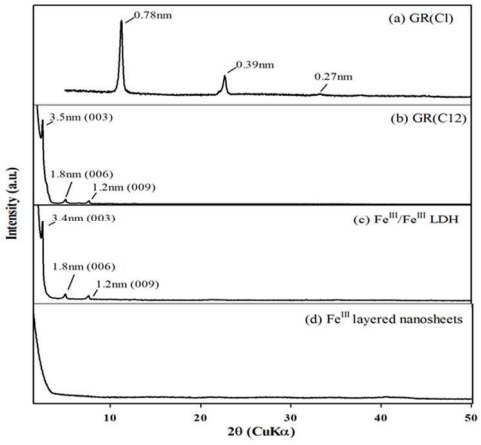

Fig. 1 XRD diffractograms of (a) GR(Cl), (b) GR(C12), (c) Fe^{III}/Fe^{III} LDH intercalated with dodecanoate, and (d) the layered Fe^{III} nanosheets.

The chloride form of GR (GR(Cl)) was initially synthesized. The chemical composition analysis indicates that the ratio of Fe^{II}/Fe^{III} is about 3.2 (Table S2), in line with the ideal ratio of 3 and previous study [26]. As shown in Fig.1(a), the XRD pattern of the as-synthesized GR(Cl) exhibits intense basal reflections with a d-spacing of 0.78 nm, in line with previous findings [26-27]. After further anion exchanging with dodecanoate anions, the XRD pattern systematically shifts to lower angular range (Fig. 1(b)). This is due to the swelling of the Fe^{II}/Fe^{III} iron hydroxide sheets to a d-spacing of 3.5 nm, as a result of successful intercalation of dodecanoate anions into layers. The trivial content of Cl within the obtained GR(C12) implies the high purity of the GR(C12), as a result, the high purity of the obtained Fe^{III}/Fe^{III} LDH in the following process of oxidation (Table S2; supplemental document S2). The similar XRD pattern for GR(C12) was also reported by using direct one-pot synthesis method [23]. Additionally, the FT-IR spectrum further confirm the intercalation of dodecanoate anions into the interlayers, where shows strong C–H vibrations (2950–2850 cm^{-1}) and COO^- vibrations (1567–1451 cm^{-1}) for GR(C12) (Fig.2(b)).

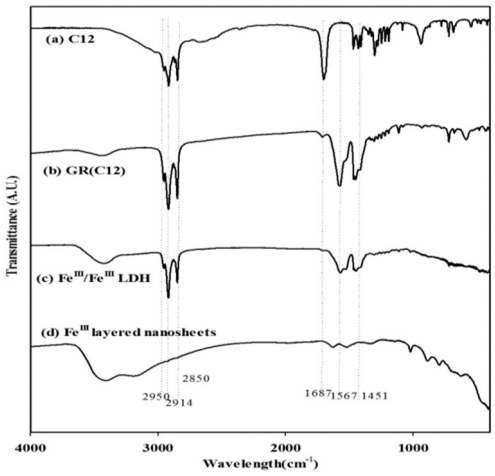

Fig. 2 The FTIR spectra of (a) dodecanoate acid (C12), (b) Fe^{III}-C12, (c) Fe^{III} /Fe^{III} LDH, and (d) the Fe^{III} layered nanosheets.

3.2 Fe^{III}/Fe^{III} LDH and exfoliation to layered Fe^{III} nanosheets

Through solid state oxidation process, the greenish blue GR(C12) particles gradually turns to orange-yellow color, indicating full oxidation of Fe^{II} to Fe^{III} within GR(C12). Meanwhile, according to Fig.1(c), the XRD for the fully oxidized product shows the similar pattern as that for GR(C12), consequently, demonstrating the preservation of the layered structure of the Fe^{III}/Fe^{III} LDH. This is in accordance with our previous studies by using one-pot synthesis [22]. The infrared analysis of Fe^{III}/Fe^{III} LDH shows C-H and COO^- vibrations consistent with those for GR(C12) (Fig.2). This demonstrates that the electrostatic interaction between interlayered dodecanoate anions and iron (ox)hydroxide sheets is still intact after full oxidation of GR(C12) [22]. The SEM and TEM images (Fig. 3a & c) for the oxidized product Fe^{III}/Fe^{III} LDH depict nice hexagonal platy shape in analogy with other LDHs [8]. The EDS analysis shows the elemental composition within Fe^{III}/Fe^{III} LDH consists of mainly C, O and Fe (Fig. S1). As shown in Fig. 3, the selected area electron diffraction (SAED) of the Fe^{III}/Fe^{III} LDH exhibits

typical hexagonal spots with a calculated lattice constant a = 0.25 nm, which indicates a highly ordered structure within the platelets (*ab* plane). The double spots at each location can be ascribed to diffractions from overlapping layers with different orientations. These evidences indicate the successful synthesis of highly crystalline structures of double layered Fe^{III} (ox)hydroxides. This is new in comparison with a previous study showing that the layered structure of GR(CO_3) was damaged after rapid oxidation by hydrogen peroxide [28].

The Fe^{III}/Fe^{III} LDH was further exfoliated to the Fe^{III} nanosheets by treating with base and ethanol washing to remove dodecanoate anions, which is confirmed by chemical analysis and EDS analysis as given in Fig. S1 and Table S2. The XRD pattern clearly shows that all basal reflections are disappeared due to disorientation at *c*-axis of stacking layers by means of dodecanoate ions removal (Fig. 1(d); Table S2). After exfoliation no crystalline iron oxides impurity was observed as seen from the XRD pattern (Fig. 1). The FT-IR spectrum of the Fe^{III} nanosheets also reveals the removal of dodecanoate anions, subsequently, the complete exfoliation of Fe^{III}/Fe^{III} LDH into nanosheets. It suggests that deprotonation of hydroxyl groups on the Iron (III) (oxy)hydroxide layers leads to repulsion and elimination of dodecanoate interlayer anions, finally achieving exfoliation of Fe^{III}/Fe^{III} LDH [22]. The TEM image (Fig. 3d) displays that the exfoliated Fe^{III} nanosheets are present as tabulate particles (Fig. 3(d)). The SAED shows a similar electron diffraction pattern as its precursor Fe^{III}/Fe^{III} LDH, which suggests its in-plane crystalline structure with highly ordered structure in *ab* planes in line with evidence from other exfoliated LDHs [7, 29]. This further demonstrates that the as-prepared Fe^{III} nanosheets via anion exchange approach shows consistent crystalline structure with that synthesized via one-pot method. Moreover, the AFM image (Fig. 3e) shows that the obtained layered Fe^{III} nanosheets constantly have an average height of about 1 nm which is about 2 times of theoretic thickness of 0.48 nm for a single layered LDH. The excess of the thickness measured by AFM has also been observed in our previous study [22]. We suggested that this can be due to the strong hydration of the layered Fe^{III} nanosheet, subsequently, causing the presence of a layer of adsorbed water molecules on the surface of the iron oxides. The TGA analysis shows the weight of the layered Fe^{III} nanosheets remains stable at over 250 °C, indicating the loss surface water associated with the solid, while the weight loss of the Fe^{III}/Fe^{III} LDH continues at over 600 °C probably due to the additional removal of dodecanoate groups within the interlayers of the Fe^{III}/Fe^{III} LDH (Fig. 4). The maximum yield of the layered Fe^{III} nanosheets product in our trials is about 0.2 kg, and can be still further scaled up to a larger quantity level. This is the advantage of using this new upscale method other than one-pot synthesis with a maximum yield of 0.4 g (Details have been specified in supplemental document S2).

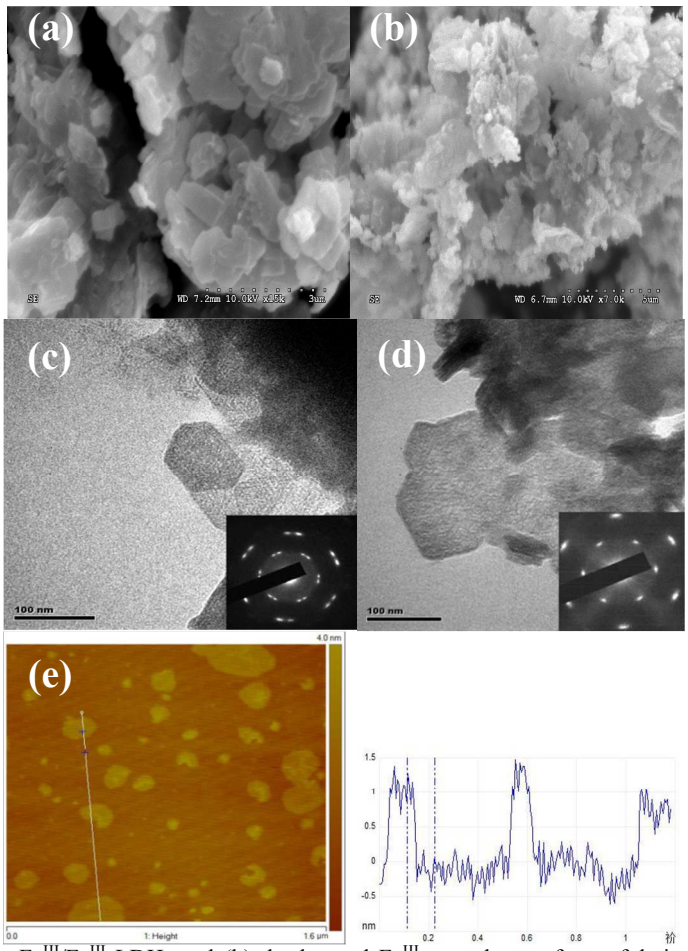

Fig. 3 (a) The SEM images of the Fe^{III}/Fe^{III} LDH, and (b) the layered Fe^{III} nanosheets after exfolation; (c) The TEM images of the Fe^{III}/Fe^{III} LDH, and (d) the exfoliated layered Fe^{III} nanosheets; (e) the AFM image and the corresponding height profile for the marked line in the image for the synthesized Fe^{III} nanosheets mapped in tapping mode.

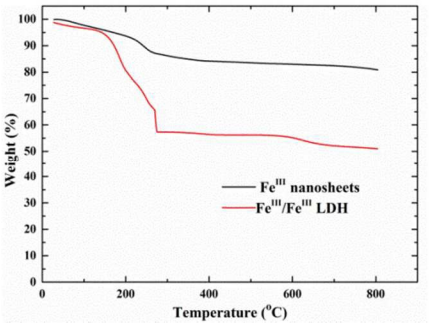

Fig. 4 TGA analysis of the Fe^{III}/Fe^{III} LDH and its exfoliated layered Fe^{III} nanosheets.

3.3 Phosphate removal by Fe^{III} nanosheets

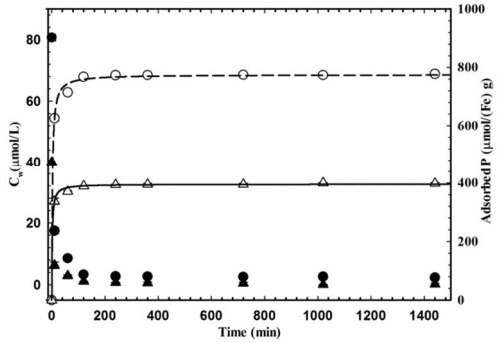

Fig. 5 Pseudo second order model fitted adsorption kinetics of phosphate towards the Fe^{III} nanosheets in 0.1M $NaNO_3$ medium at pH 7.0 with initial concentrations of 40 μmol/L (▲ and Δ) and 80 μmol/L (● and ○). The solid content of the Fe^{III} nanosheets is 0.1 g/L. The dash and solid curves were obtained by fitting adsorption data with pseudo-second-order equation (Eq.1).

Fig. 5 shows that phosphate adsorption to Fe^{III} nanosheets is time dependent, and the adsorption kinetics can be well described by pseudo-second order model (Eq.1).

$$q_t = \frac{k_2 q_e^2 t}{1+k_2 q t} \quad \text{(Eq.1)}$$

where q_t is the amount of adsorbed phosphate on the Fe^{III} nanosheets at any time t (μmol/g), k_2 and q_e denotes the rate constant of phosphate adsorption (g/ (μmol min)), and the amount of adsorbed phosphate on adsorbent at equilibrium time (μmol/g), respectively. The phosphate adsorption appears rather quick and efficient with an adsorption constant k_2 ranging from 5.2×10^{-4} to 1.4×10^{-3} g/(μmol min) for the initial concentrations of 40 and 80 μmol/L (1.24 to 2.4 mg P/L) at pH 7.0, and maxima adsorption of 396 and 775 μmol/g can be reached within 1 hour. On the other hand, our results show that only a dosage of 0.1 g/L is sufficient to remove excess phosphate of 80 μmol/L (2.4 mg P/L) from water.

The phosphate adsorption isotherms by the synthesized Fe^{III} nanosheets can be successfully fitted by Langmuir model with R^2 ranging from 0.945 to 0.988 (Eq.2)

$$C_s = \frac{K_L C_{max} C_w}{1+K_L C_w} \quad \text{(Eq.2)}$$

where C_s (μmol/g) and C_w (μmol/L) represent the adsorbed phosphate on Fe^{III} nanosheets and free phosphate concentration in aqueous phase; K_L and C_{max} are Langmuir adsorption affinity and phosphate adsorption capacity by Fe^{III} nanosheets.

Table 1 Langmuir isotherm parameters for phosphate adsorption to the Fe^{III} nanosheets at three different pHs

pH	$NaNO_3$ (mol/L)	K_L(L/μmol)	C_{max}(μmol/g)	R^2
5.0	0.1	0.02 ± 0.01	2540 ± 92	0.983
	0	0.03 ± 0.01	2497 ± 104	0.953
7.0	0.1	0.02 ± 0.01	1502 ± 81	0.946
9.0	0.1	0.06 ± 0.02	868 ± 41	0.988

The phosphate adsorption to the Fe^{III} nanosheets materials were performed at pH 5.0, 7.0 and 9.0, respectively. The results reveal that the maximum adsorption capacity of phosphate to the Fe^{III} nanosheets materials can reach up to 2540 μmol/g depending on pH (Table 1; Fig. 6a), which shows much higher phosphate adsorption than to poor crystalline goethite (270 μmol/g), lepidocrocite (270 μmol/g), akaganeite (450 μmol/g) and iron bearing LDH (1450 μmol/g) particles (Table 2) from previous works [1-2, 30], and slightly higher than that 2490 μmol/g for amorphous ferrihydrite which is generally considered as most efficient iron adsorbent for phosphate removal [31]. This may be attributed to the relatively higher surface area (185 m^2/g) for the Fe^{III} nanosheets materials than those poor crystalline iron oxides. The phosphate adsorption of the exfoliated Fe^{III} nanosheets remarkably increases in comparison to 605 μmol/g at pH 5.0 of its precursor Fe^{III}/Fe^{III} LDH with dodecanoate ions intercalated (Table 2; figure not shown), and the analogous layered materials Mg/Fe LDH (Table 2). The notable enhance of the phosphate adsorption towards phosphate is probably due to the result of releasing more inaccessible adsorption sites between interlayers [32]. By normalizing the phosphate adsorption to iron content, the ratio of adsorbed phosphate to Fe (P/Fe) of 4006 μmol/(g Fe) for the layered Fe^{III} nanosheets is significantly higher than that of 3761 μmol/(g Fe) due to slightly high iron content of ferrihydrite (Table 2). However, the notable high P/Fe of 6444 μmol/(g Fe) for Mg/Fe LDH cannot be accounted for, since both Mg and Fe are responsible for the removal of phosphate [1].

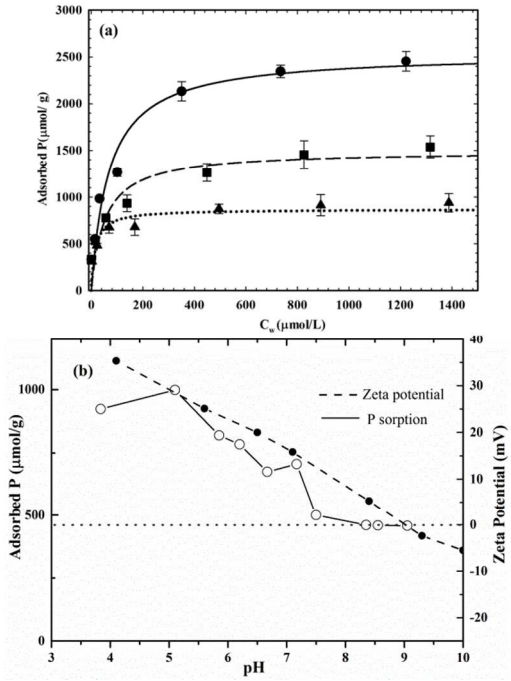

Fig. 6 (a) Adsorption isotherms of phosphate to the Fe^{III} nanosheets material at pH 5.0(●), 7.0 (■) and 9.0 (▲). Each

adsorption isotherm was fitted using all raw data obtained in triplicates (n = 21). Data points refer to averages of triplicates, vertical bars represent standard deviation (n = 3); (b) pH adsorption edge of phosphate towards the layered Fe^{III} nanosheets (left y-axis), along with zeta potential of the layered Fe^{III} nanosheets (right y-axis) in a pH range of 3 to 10. The dosage of adsorbent is 0.1 g/L, while the initial concentration of phosphate is 150 μmol/L.

Table 2 Comparison of the adsorption capacities of different adsorbents for removing phosphate

Adsorbent	pH	Fe (%) [a]	BET surface area (m^2/g)	Max. P (μmol/g)	P/Fe (μmol/g)	Ref.
Fe^{III} nanosheets	5	63.4	185	2540	4006	This study
Fe^{III} nanosheets	7	63.4		1522	2401	This study
Fe^{III}/ Fe^{III} LDH	5	37.2	32	605	1626	This study
Goethite	5	62.9	63	270	429	2
Akaganeite	5	55.8	94	450	806	2
lepidocrocite	5	62.9	85	270	429	2
Granulated ferric hydroxide	5.5	55.8	280	770	1380	30
Ferrihydrite	6	66.2	187	2490	3761	31
Mg/Fe-LDH	6	22.5	NA [b]	1450	6444	1

[a] The iron contents of the Fe^{III}/Fe^{III} LDH and Fe^{III} nanosheets were retrieved from Table S2; the iron contents of goethite, akaganeite, lepidocrocite, granulated ferric hydroxide (100% akaganeite) and ferrihydrite were obtained from Mineralogy database [33], while the iron content for Mg/Fe-LDH was calculated based on the formula of $Mg_2Fe(OH)_5CO_3$. [b] NA: not available.

As depicted in Fig. 6a&b, the phosphate adsorption by the Fe^{III} nanosheets materials decreases with the increase of pH from 3 to 10. It is well known that phosphate ion can present in different states according to its $pK_{a,1}$ of 2.15, $pK_{a,2}$ of 7.20 and $pK_{a,3}$ of 12.33 [16]. Hence, the predominated fraction is $H_2PO_4^-$ (approximately 100%) at pH 5, while HPO_4^{2-} ion almost 100% dominates at pH 9. Nevertheless, the surface of the Fe^{III} nanosheets appears to be less positive charge, and finally becoming negatively charged at higher pH (Fig. 6b), consequently, causing greater electrostatic repulsion to the more negatively charged HPO_4^{2-}. This is in agreement with previous finding by Chitrakar and coworkers [34].

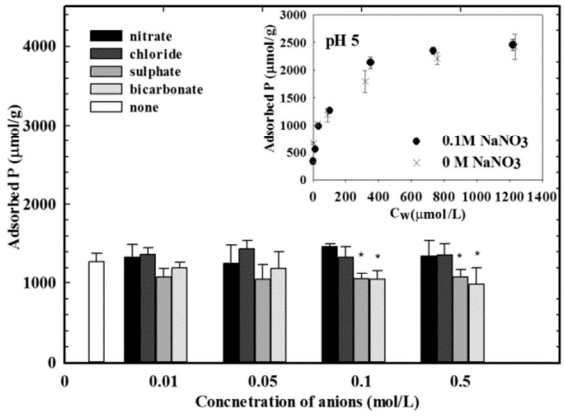

Fig. 7 Influence of different anions on the adsorption of phosphate to the layered Fe^{III} nanosheets in comparison with that without addition of background electrolyte at pH 7.0. The insert is the adsorption isotherms of phosphate to SSI in the presence (●) and absence (×) of 0.1M $NaNO_3$ at pH 5.0. Asterisks indicate that the phosphate adsorption are significant different from that without addition of electrolyte ($p < 0.05$).

Anions such as NO_3^-, Cl^-, SO_4^{2-} and CO_3^{2-} are ubiquitous inorganic ligands in the environment, which may affect the efficiency of the phosphate removal. Thereby, the influence of those anions on the removal of phosphate was further investigated in this study. As illustrated in Fig. 7, the removal of phosphate by the Fe^{III} nanosheets slightly increases in the presence of the monovalent anions NO_3^- or Cl^- with concentrations up to 0.5 M at pH 7 (PO_4^{2-}/X^{n-} up to 2000, X represents coexisted anions), which may imply the phosphate adsorbed via inner-sphere association in line with previous finding of phosphate sorption to other iron oxyhydroxides [35-36]. However, the higher positive charge for phosphate seems not the only reason causes the favorable binding of phosphate with the iron oxide according to the sorption comparison with/without adding nitrate ions at pH 5 where almost 100% of phosphate ions exist as monocharged $H_2PO_4^-$ (Fig. 7). The addition of the bivalent anions SO_4^{2-} or CO_3^{2-} (presents as HCO_3^-) up to 0.05 M leads to the slightly decrease of the phosphate removal, but not statistically significant ($p > 0.05$; $PO_4^{2-}/X^{n-} \leq 200$), whereas, a significant decrease of the phosphate adsorption at higher concentration (0.1 to 0.5 M), indicating the strong competition of SO_4^{2-} or CO_3^{2-} (presents as HCO_3^-) ions with phosphate binding with the Fe^{III} nanosheets materials. The similar observation was reported in phosphate adsorption by amorphous granulated ferric hydroxide [30], indicating that the iron bearing materials such as the Fe^{III} nanosheets have strong selectivity to adsorb phosphate, as a consequence, can be considered as ideal adsorbent for removing phosphate ions from water.

3.4 XPS surface analysis

The high resolution spectra of O 1s, Fe 2p and P 2p for the Fe^{III} nanosheets materials before and after reaction with phosphate are given in Fig. 8. The XPS analysis shows notably change of the O 1s spectra before and after loading phosphate at pH 5 (Fig. 8a). By peak fitting by three different components at ~529.8 eV, ~531.0 eV and ~532.8 eV corresponding to O-Fe bonding, OH/O-P bonding, and adsorbed water, respectively, the O 1s spectra clearly show the significant increase of the binding energy at ~531.0 eV to that at 529.8 eV as a result of phosphate loading. Even though it is difficult to identify the binding energy of OH in Fe^{III} nanosheets from that of O-P [35], the enhanced relative intensity at ~531 eV to that at 529.8 eV can be due to binding of phosphate to O-Fe, subsequently leading to the

formation of Fe-O-P bonding. This is similar to our previous findings on the O 1s spectra for the SO_4^{2-} loaded Fe^{III}/ Fe^{III} LDH [22], and phosphate adsorption to ferrihydrite [35]. In addition, Fe 2p spectra are almost identical before and after loading phosphate, suggesting that Fe atoms do not directly participate in phosphate adsorption to form Fe-P bonding (Fig. 8b). The appearance of P 2p spectra at binding energy of ~133.4 eV after phosphate adsorption indicates the successful phosphate loading on the Fe^{III} nanosheets (Fig. 8c). Interestingly, the binding energy of ~133.4 eV observed for phosphate on the Fe^{III} nanosheets is very similar to that of 133.6 eV for $FePO_4$ reference and phosphate adsorbed ferrihydrite [35], which can further confirm the assumption of the formation of Fe-O-P bonding obtained in O 1s spectra. The significant increase of the XPS intensity of P 2p signal with the pH decreasing from 7.0 to 5.0 is in agreement with the increased adsorption of phosphate by the Fe^{III} nanosheets as pH decreases (Fig. 6; Table 1). The XPS analyses of the O 1s, Fe 2p and P 2p spectra provide spectroscopic evidence for phosphate adsorption to the Fe^{III} nanosheets by forming inner-sphere complex of the Fe-O-P type. However, the overlapping of the binding energies of O-H with O-P peaks (Fig. 8b), hinders to further distinguish the binding of phosphate with the synthesized iron oxide by means of monodentate from bidentate complexation, which needs to be investigated in future work.

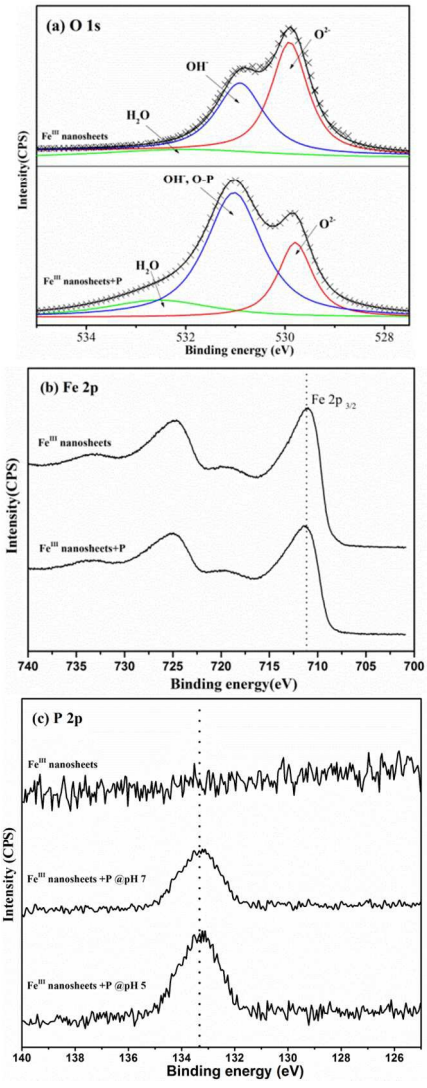

Fig. 8 (a) O 1s and (b) Fe 2p spectra of the Fe^{III} nanosheets before and after reaction with 250 µmol/L phosphate at pH 5, respectively; (c) P 2p spectra of the Fe^{III} nanosheets before and reaction with 250 µmol/L phosphate at pH 5 and pH 7, respectively.

4. Conclusions

In this work, an upscale facile method was successfully developed for synthesis of the layered Fe^{III} nanosheets material by means of anion exchange, solid-state oxidation and exfoliation. Its structure was well characterized by means of XRD, FT-IR, AFM, TGA, XPS, and electronic microscopies. Our results confirm that the as-synthesized Fe^{III} nanosheets material exhibits good crystallinity, high BET surface area (185 m^2/g) with layered structure. Our study further demonstrate that the synthesized layered Fe^{III} nanosheets material can strongly and rapidly adsorb phosphate ions which are considered to be the main pollutant causing eutrophication in lake and seawater. The maxima adsorption of phosphate by the Fe^{III} nanosheets are up to 2540 µmol P/g (4006 µmol P/g Fe) depending on pH, which are considerably higher those by other crystalline iron oxides such as goethite and lepidocrocite. In addition, the data suggest that the layered Fe^{III} nanosheets show strong adsorption selectivity towards phosphate even in the presence of high concentrations of background ions such as SO_4^{2-}, NO_3^- and CO_3^{2-} up to 0.05 M. XPS surface analysis clearly shows the binding of P atoms with the layered Fe^{III} nanosheets material and the formation of inner-sphere complex in Fe-O-P bonding. Overall, the successfully synthesized layered Fe^{III} nanosheets material is considered as cost-effective, environmental friendly and highly efficient adsorbent for removing phosphate pollutant from eutrophic water, which can be further used as coating material of filter bed in water treatment technologies.

Acknowledgements

The current work was financially supported by the National Basic Research Program of China (973 Program, Grant No. 2011CB933704), the National Natural Science Foundation of China (Grant No. 21407131), and the Fundamental Research Funds for the central University, China University of Geosciences (Wuhan) (CUG150602)

Notes and references

[a] *Department of Chemistry, Faculty of Material Sciences and Chemistry, China University of Geosciences, Wuhan 430074, China. Tel: +86-027-67883739; E-mail: jegerfang@gmail.com*
[b] *Department of Plant and Environmental Sciences, University of Copenhagen, Thorvaldsensvej 40, DK-1871 Frederiksberg C, Denmark*
[c] *Sino-Danish Centre for Education and Research (SDC)*
[d] *State Key Laboratory of Environmental Aquatic Chemistry, Research Centre for Eco-Environmental Sciences, Chinese Academy of Sciences, Beijing 100085, China; E-mail: wgds@rcees.ac.cn*

1 J. Das, B. S. Patra, N. Baliarsingh and K. M. Parida, *Appl. Clay Sci.*, 2006, **32**, 252-260.
2 J. Kim, W. Li, B. L. Philips and C. P. Grey, *Energy Environ. Sci.*, 2011, **4**, 4298-4305.
3 K. Mandel, A. Drenkova-Tuhtan, F. Hutter, C. Gellermann, H. Steinmetz and G. Sextl, *J. Mater. Chem. A*, 2013, **1**, 1840-1848.
4 J. Yang, L. Zhou, J. Zhang, J. Zou, Z. Yuan and C. Yu, *Chem.-Eur. J.*, 2013, **19**, 5578-5585.
5 I. Emmanuelawati, J. Yang, J. Zhang, H. Zhang, L. Zhou and C. Yu, *Nanoscale*, 2013, **5**, 6173-6180.

6 J. Yang, L. Zhou, L. Zhao, H. Zhang, J. Yin, G. Wei, K. Qian, Y. Wang and C. Yu, *J. Mater. Chem.*, 2011, **21**, 2489-2494.
7 Q. Wang and D. O'Hare, *Chem. Rev.*, 2012, **112**, 4124-4155.
8 J. He, M. Wei, B. Li, Y. Kang, D. Evans and X. Duan, in *Layered Double Hydroxides*, eds. X. Duan and D. Evans, Springer Berlin Heidelberg, 2006, 89-119.
9 K. Okamoto, T. Sasaki, T. Fujita and N. Iyi, *J. Mater. Chem.*, 2006, **16**, 1608-1616.
10 D. G. Evans and X. Duan, *Chem. Comm.*, 2006, 485-496.
11 K. H. Goh, T. T. Lim and Z. Dong, *Water Res.*, 2008, **42**, 1343-1368.
12 K. Kuzawa, Y.-J. Jung, Y. Kiso, T. Yamada, M. Nagai and T.-G. Lee, *Chemosphere*, 2006, **62**, 45-52.
13 Y. Seida and Y. Nakano, *Water Res.*, 2002, **36**, 1306- 1312.
14 Y. You, G. F. Vance and H. Zhao, *Appl. Clay Sci.*, 2001, **20**, 13-25.
15 R. L. Goswamee, P. Sengupta, K. G. Bhattacharyya and D. K. Dutta, *Appl. Clay Sci.*, 1998, **13**, 21-34.
16 H. He, H. Kang, S. Ma, Y. Bai and X. Yang, *J. Colloid Interf. Sci.*, 2010, **343**, 225-231.
17 N. Khare, J. D. Martin and D. Hesterberg, *Geochim.Cosmochim. Ac.*, 2007, **71**, 4405-4415.
18 P. Refait and J. M. R. Génin, *Corros. Sci.*, 1993, **34**, 797-819.
19 H. C. B. Hansen, *Clay Miner.*, 1989, **24**, 663-669.
20 L. Legrand, L. Mazerolles and A. Chausse, *Geochim.Cosmochim. Ac.*, 2004, **68**, 3497-3507.
21 P. Refait and J. M. R. Genin, *Corros. Sci.*, 1993, **34**, 2059-2070.
22 L. Huang, L. Fang, T. Hassenkam, K. N. Dalby, K. G. Scheckel and H. C. B. Hansen, *J. Mate. Chem. A*, 2013, **1**, 13664-13671.
23 K. B. Ayala-Luis, C. B. Koch and H. C. B. Hansen, *Applied Clay Science*, 2010, **50**, 512-519.
24 B. Ayala-Luis, C. B. Koch and H. C. B. Hansen, *Appl. Clay Sci.*, 2010, **48**, 334-341.
25 L. Heiberg, T. V. Pedersen, H. S. Jensen, C. Kjaergaard and H. C. B. Hansen, *J. Environ. Qual.*, 2010, **39**, 734-743.
26 H. C. B. Hansen, S. Guldberg, M. Erbs and C. Bender Koch, *Appl. Clay Sci.*, 2001, **18**, 81-91.
27 P. Refait and J. M. R. Genin, *Corros. Sci.*, 1993, **34**, 797-819.
28 C. Ruby, C. Upadhyay, A. Géhin, G. Ona-Nguema and J. M. R. GÉnin, *Environm. Sci. Technol.*, 2006, **40**, 4696-4702.
29 R. Ma, Z. Liu, K. Takada, N. Iyi, Y. Bando and T. Sasaki, *J. Am. Chem. Soc.*, 2007, **129**, 5257-5263.
30 A. Genz, A. Kornmüller and M. Jekel, *Water Res.*, 2004, **38**, 3523-3530.
31 Y. T. Liu and D. Hesterberg, *Environm. Sci. Technol.*, 2011, **45**, 6283-6289.
32 Z. P. Liu, R. Z. Ma, M. Osada, N. Iyi, Y. Ebina, K. Takada and T. Sasaki, *J. Am. Chem. Soc.*, 2006, **128**, 4872-4880.
33 D. Barthelmy, The Mineralogy Database, http://webmineral.com/, Accessed Feb. 5th, 2015.
34 R. Chitrakar, S. Tezuka, A. Sonoda, K. Sakane, K. Ooi and T. Hirotsu, *J. Colloid Interf. Sci.*, 2006, **298**, 602-608.
35 M. Mallet, K. Barthélémy, C. Ruby, A. Renard and S. Naille, *J. Colloid Interf. Sci.*, 2013, **407**, 95-101.
36 G. Zhang, H. Liu, R. Liu and J. Qu, *J. Colloid Interf. Sci.*, 2009, **335**, 168-174.